

Shape-Memory Semicrystalline Polymeric Materials Based on Various Rubbers

Ozge Akca and Oguz Okay*

A simple strategy is presented for the fabrication of shape-memory materials containing commercial rubbers including natural rubber, *cis*-polybutadiene, and styrene-butadiene rubber. Dissolution of the rubbers in *n*-octadecyl acrylate (C18A) monomer followed by UV polymerization at 30 °C leads to the formation of interconnected interpenetrating polymer networks (c-IPNs) possessing crystalline domains. They exhibit melting (T_m) and crystallization temperatures (T_{cry}) between 45–50 and 35–40 °C, respectively, that can be tuned by the amount and the type of the rubbers. All c-IPNs exhibit a significant temperature sensitivity in their viscoelastic and mechanical properties when the temperature is changed between below and above T_m and T_{cry} . The morphology of c-IPNs consists of amorphous nanoparticles of around 64 nm diameter composed of interconnected noncrystalline poly(C18A) (PC18A) and rubber networks, surrounded by crystalline PC18A segments. c-IPNs exhibit tunable mechanical properties, for example, their Young's modulus and toughness can be varied between 8.3–73 MPa, and 1.9–23 MJ·m⁻³, respectively, by changing the amount and type of the rubber. Because of the coexistence of chemical cross-links and crystalline domains acting as the netpoints and switching segments, respectively, c-IPNs exhibit an efficient shape-memory function as demonstrated by their potential application as a robotic gripper.

instance, Kuang et al recently reported a 3D printing ink composed of urethane diacrylate and a semicrystalline polymer for printing a stretchable shape-memory and self-healing semi-IPN elastomer.^[6] Moreover, generating these smart functions in commercially available and widely used rubbers draw much attention in recent years.^[7] Ionically modified commercial rubbers, interpenetrating polymer networks (IPNs), and polymer blends based on various rubbers have been prepared exhibiting self-healing and/or shape-memory functions.^[8–20] Du et al reported a shape-memory polymer composite consisting of a polyolefin elastomer, and stearic acid displaying two thermal transitions when melt-mixed with the elastomer.^[21]

We recently reported a simple strategy for producing self-healing and shape-memory interconnected IPNs (c-IPNs) based on butyl rubber (IIR) containing 1.7 ± 0.2 mol% isoprene units, and semicrystalline poly(*n*-octadecyl acrylate) (PC18A).^[22] Dissolving IIR in liquid *n*-octadecyl acrylate (C18A) monomer followed by UV polymerization at ambient

temperature using a photoinitiator results in c-IPNs with tunable mechanical properties and high self-healing and shape-memory efficiencies. The lamellar crystals with a melting temperature T_m of around 50 °C formed by octadecyl side chains of PC18A act as physical cross-links and constitute most of the effective cross-links in c-IPNs, and are responsible for their smart functions. The advantage of our strategy as compared to smart IPNs and polymer blends reported before is the solvent-free preparation of c-IPNs at ambient temperature without rigorous mixing of the reaction components.

Our aim in the present study was to understand how the degree of unsaturation of the commercial rubber affects the thermal and mechanical properties, and smart functions of the c-IPNs. We conducted experiments with natural rubber, *cis*-polybutadiene, and styrene-butadiene rubber having a much higher unsaturation degree than IIR. As will be seen below, increasing the degree of unsaturation of the rubber increases the chemical cross-link density of the resulting c-IPNs, and significantly improves their mechanical properties. Moreover, an interesting behavior was observed in that c-IPNs above T_m with a low stiffness (kPa level) exhibit a more elastic character than those below T_m with a high stiffness (MPa level). Although the self-healing ability of c-IPNs disappears by replacing IIR with the

1. Introduction

Self-healing and shape-memory polymers of high mechanical strength attract significant interest in the past decade.^[1–3] The ability of synthetic polymers to heal damage autonomously or under the effect of an external stimulus will improve their service lifetime, environmental impact, and energy efficiency. Moreover, shape-memory is the capability of a material to adopt various shapes and recover the original shape under the effect of a stimulus. These unique features of self-healing and shape-memory polymers make them attractive materials for numerous applications including implants, actuators, sensors, superconducting devices, smart medical devices, and flexible electronics.^[1,3–5] For

O. Akca, O. Okay
 Department of Chemistry
 Istanbul Technical University
 Maslak, Istanbul 34469, Turkey
 E-mail: okay@itu.edu.tr

 The ORCID identification number(s) for the author(s) of this article can be found under <https://doi.org/10.1002/mame.202100776>

DOI: 10.1002/mame.202100776

Table 1. The number-average molecular weights \bar{M}_n , polydispersity indices (PDI), and unsaturation degrees of the rubbers used in the c-IPN preparation (see also Figures S2–S4, Supporting Information).

Rubber	Code	\bar{M}_n [kDa]	PDI	Unsaturation [mol%]
Butyl rubber, BK-1675N	IIR	320	2.1	1.7
Natural rubber, RSS 3	NR-1	506	3.1	100
Natural rubber, SVR-3L	NR-2	418	4.2	100
Polybutadiene rubber, CBR-1220	CBR	232	3.3	99
Styrene-butadiene rubber, SBR-1502	SBR	229	3.9	84

other rubbers due to the increasing number of chemical cross-links, they all exhibit a strong shape-memory function, as demonstrated for the use as a thermoresponsive soft robotic gripper.

2. Experimental Section

2.1. Materials

Four different commercial rubbers were used in the experiments. Two natural rubbers, namely Vietnam natural rubber (SVR-3L), and ribbed smoked sheets (RSS 3) were purchased from Viet Phu Think Rubber Joint Stock Co. Polybutadiene rubber with a cis-content of 97 wt% (CBR-1220) and styrene-butadiene rubber (SBR-1502) were obtained from Takht-E-Jamshid Petrochem. Co, Iran and HIP Petrohemija Ad Panvec, Serbian, respectively. Butyl rubber (BK-1675N) used for comparison was obtained from Nizhnekamskneftekhim Co., Russia, and has an unsaturation degree of 1.7 ± 0.2 mol%.^[22] It had to be noted that two additional rubbers, namely acrylonitrile-butadiene rubber (615B, Songhan Plastic Tech. Co. Ltd., China) and ethylene-propylene-diene monomer (Keltan-4869, Arlanxeo, The Netherlands) were also selected as the rubber components of c-IPNs. However, preliminary experiments showed that they are insoluble in C18A monomer so that they cannot be used in the IPN preparation. For the purification of the rubbers, they were first dissolved in toluene at a concentration of around 5% w/v and then precipitated in methanol finally dried under vacuum to constant weight. Their purities and unsaturation degrees were checked by ATR-FTIR (Agilent Technologies Carry 63) and ¹H-NMR (Agilent VNMRS 500 MHz) (Figures S1–S4, Supporting Information). The molecular weight of the rubbers was determined on a gel permeation chromatograph (Malvern GPC Max, RI detector, mobile phase: THF) using polystyrene standards (PolyCal, Malvern). **Table 1** shows the number-average molecular weight \bar{M}_n , polydispersity index (PDI), and the unsaturation degree of the rubbers used in the c-IPN preparation. Other chemicals, namely n-octadecyl acrylate (C18A), 2-hydroxy-4'-(2-hydroxyethoxy)-2-methylpropiophenone (Irgacure 2959) were purchased from Sigma Aldrich (St. Louis, MO) and used as received.

2.2. c-IPN Preparation

c-IPNs based on rubber and PC18A were prepared by in situ bulk photopolymerization of C18A at 30 ± 2 °C in the presence

Table 2. Synthesis parameters of c-IPNs.

Rubber [wt%]	Rubber [g]	C18A [g]	Irgacure 2959 [mg]
0	0	5	10
20	1	4	8
30	1.5	3.5	7
40	2	3	6

of rubber and Irgacure 2959 initiator (0.20 mol% with respect to C18A) under UV light at 360 nm. Typically, to prepare a c-IPN with 20 wt% rubber, 1 g of rubber was dissolved in 4 g of C18A for 8 h at 80 °C, which is above the melting temperature of C18A (30 °C). After cooling to 30 °C, Irgacure 2959 (8 mg) was added to the homogeneous and transparent rubber-C18A melt mixture. After stirring at 60 rpm for 30 min, the mixture was cast between two PVC slides and the photopolymerization was conducted under UV light for 1 h at 30 ± 2 °C. The rubber content could be increased up to 40 wt% because of the high viscosity of the mixture at higher rubber concentrations preventing homogeneity. The synthesis parameters of c-IPNs are compiled in **Table 2**.

2.3. Characterization

The melting (T_m) and crystallization temperatures (T_{cr}) of c-IPNs were measured using differential scanning calorimetry (DSC) on a Perkin Elmer Diamond DSC instrument under nitrogen purge. The specimens in DSC hermetic pans were subjected to heating-cooling cycles between 5 and 80 °C at a rate of 5 °C·min⁻¹. From the melting enthalpy (ΔH_m), the degree of crystallinity f_{cr} was estimated as $f_{cr} = w_{C18A} \Delta H_m / \Delta H_m^0$, where w_{C18A} is the weight fraction of C18A in the melt mixture, and ΔH_m^0 is the melting enthalpy of crystalline PC18A (219.4 J g⁻¹).^[23,24] The morphologies of c-IPNs stained with UranylLess were examined by using transmission (TEM) and scanning transmission electron microscopy (STEM) on a JEOL ARM-200CF instrument at a voltage of 200 kV, as described earlier.^[22] The size distribution of the dispersed phase was determined by measuring the cross-sectional area of at least 100 particles using ImageJ software (NIH, USA), and then converting the data into sphere-equivalent diameters.^[22]

Rheological measurements were performed at both below and above T_m of c-IPNs on a Gemini 150 Rheometer system (Bohlin Instruments, Malvern) with a parallel plate geometry (diameter 20 mm) and a Peltier temperature control system. The strain amplitude was set to 0.1% to ensure a linear viscoelastic response. The uniaxial tensile mechanical performances of c-IPNs were determined on a Zwick Roell testing machine using a 1 kN load cell. Rectangular specimens with dimensions 6 cm x 1 cm x 1.5 mm and a gauge length of 5 mm were used. They were stretched at a rate of 5.0 min⁻¹ during which the nominal (engineering) stress σ_{nom} and strain ϵ (length change of the specimen/its initial length) were recorded. Young's modulus E was calculated from the slope of the initial elastic regime (between $\epsilon = 0.01$ – 2%). The toughness W , that is, the energy to break was calculated from the area under the stress–strain curve up to the break point. Cyclic tensile tests were conducted under the same stretch

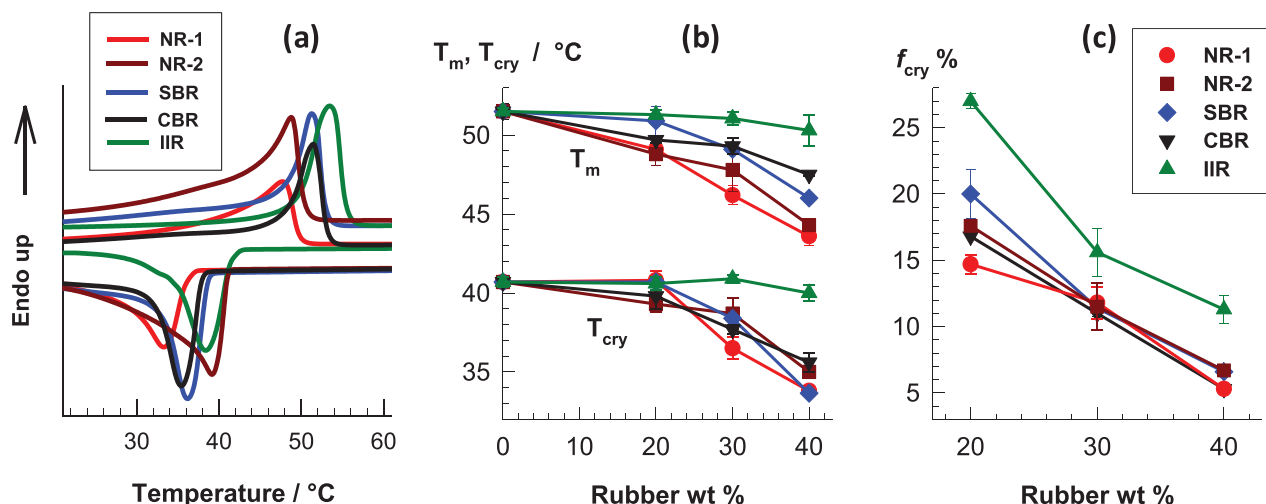


Figure 1. a) DSC scans of c-IPNs with 30 wt% rubber. Type of rubbers as indicated. b,c) The melting (T_m) and crystallization temperatures (T_{cr}), and the degree of crystallinity f_{cr} of c-IPNs plotted against their rubber contents.

rate by stretching the specimens up to 60% followed by unloading to zero stress at the same rate. At least 20 samples from each c-IPN group were measured during the tensile tests, and the results were averaged. For the determination of the swelling ratio and soluble fraction of c-IPNs, the specimens of 5 cm x 4 cm x 1.5 mm dimensions were immersed in an excess of toluene during which toluene was refreshed several times. After equilibrium swelling which required at least 2 weeks, they were immersed in methanol, and finally dried under vacuum to constant mass. The equilibrium weight swelling ratio q_w was calculated as $q_w = m_s/m_{dry}$, where m_s and m_{dry} are the masses of the specimens after equilibrium swelling, and after drying, respectively. The soluble fraction w_{sol} was calculated as $w_{sol} = 1 - m_{dry}/m_o$, where m_o is the initial mass of the specimen. The shape-memory behavior of c-IPNs was quantified by a bending test. The rectangular specimens (5 cm x 1 cm x 1.5 mm) were immersed in a water bath at 65 °C (above T_m) for 15 min, bended to a U-shape, and then immersed in a water bath at 25 °C to fix the temporary shape with a deformation angle θ_d . The shape recovery was initiated by slowly increasing the water bath temperature at 1–3 °C steps up to 75 °C during which the deformation angle θ_d was monitored using Image-Pro Plus image analyzing system. The shape-recovery ratio R_θ was calculated as $R_\theta = \theta_d/180$.

3. Results and Discussion

c-IPNs based on rubber (20 to 40 wt%) and PC18A were prepared by bulk photopolymerization of C18A monomer in the presence of four different rubbers, and Irgacure initiator at 30 ± 2 °C. The rubbers used were SBR-1502, CBR-1120, RSS-3, and SVR-3L, which are abbreviated as SBR, CBR, NR-1, and NR-2, respectively. For comparison butyl rubber (IIR) was used as a reference in the c-IPN preparation.^[22] The number-average molecular weights and the polydispersity indices of the rubbers were in the ranges of 300–500 kDa and 2.1–4.2, respectively (Table 1). Except IIR with an unsaturation degree of 1.7 mol%, all other rubbers have much higher unsaturation degrees, as compiled in Table 1.

The rubbers could easily be solubilized in liquid C18A at 80 °C to obtain a homogeneous mixture. After cooling to 30 °C and addition of Irgacure initiator (0.2 mol%), photopolymerization was conducted for 1 h to obtain c-IPNs with 20, 30, and 40 wt% rubber. All c-IPNs were opaque in appearance reflecting a phase separation during polymerization of C18A. In the following, we first discuss the microstructure and morphology of c-IPNs. The viscoelastic behavior, types of elastically effective cross-links in c-IPNs, their mechanical properties, and shape-memory functions are discussed in the following sections.

3.1. Microstructure and Morphology

Figure 1a shows DSC scans of c-IPNs containing various rubbers at a fixed amount of 30 wt%. They all exhibit melting and crystallization peaks at 45–50 and 35–40 °C, respectively, revealing formation of octadecyl (C18) side-chain crystals.^[22] The T_m and T_{cr} , and the degree of crystallinity f_{cr} of C18 side chains compiled in Figure 1b,c reveal that they all decrease as the rubber content is increased. The decrease in the transition temperatures becomes less pronounced in the order of NR-1 > NR-2 > SBR > CBR > IIR indicating that IIR with the lowest degree of unsaturation produces more thermally stable alkyl crystals as compared to the other rubbers. In accord with this finding, c-IPNs prepared using IIR exhibit the highest degree of crystallinity at all rubber contents (11–27%). We attribute this behavior to the low unsaturation degree of IIR that would produce lower number of chemical cross-links in c-IPNs compared to other rubbers. This will lead to the formation of more flexible PC18A chains facilitating the alignment of C18 side chains. As will be seen below, this explanation was supported by the viscoelastic and swelling behavior of c-IPNs.

Figure 2a,b shows TEM images of UranylLess-stained c-IPNs with 30 wt% SBR (a) and CBR (b), where the amorphous and crystalline domains appear bright and dark, respectively.^[22] The insets show the size-distribution of the bright (amorphous) regions.

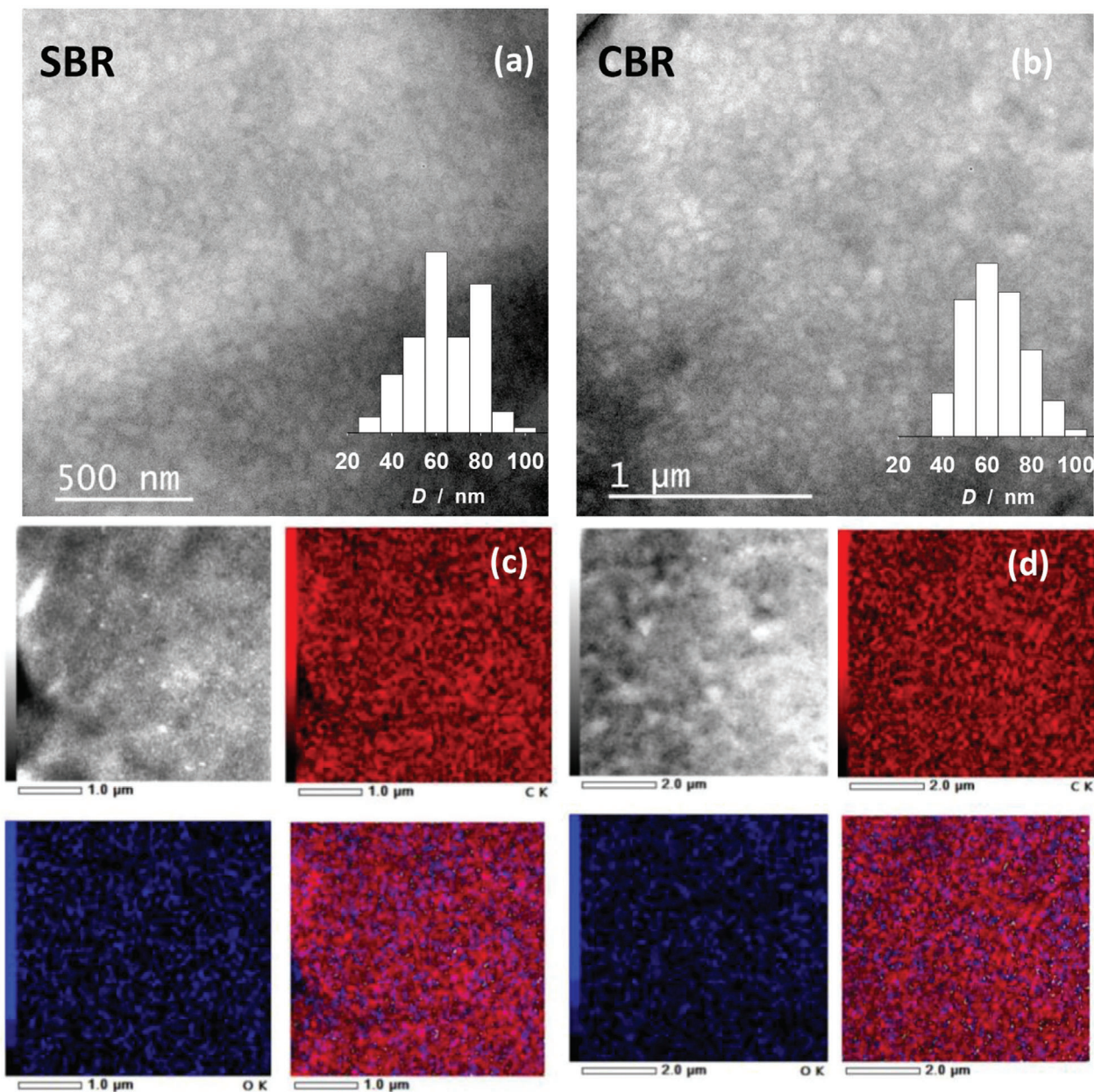


Figure 2. TEM images of c-IPNs with 30 wt% a) SBR and b) CBR. The amorphous and crystalline domains appear bright and dark, respectively. The insets show the size-distribution of the bright (amorphous) regions. Scale bars: 500 nm (a) and 1 μ m (b). STEM images of the same c) SBR and d) CBR-based c-IPNs and their EDX maps. Scale bars: 1 (c), and 2 μ m (d).

PC18A and the rubber component of c-IPNs distribute almost homogeneously over the whole investigated area. The morphology consists of amorphous regions with a number-average diameter D of 64 nm and a PDI of 1.05 surrounded by crystalline domains. Thus, the interconnected noncrystalline PC18A and rubber networks seem to form the nanosized amorphous particles surrounded by the crystalline PC18A segments. This is in contrast to the c-IPNs formed using IIR rubber where the crystalline domains of 500–800 nm in diameter are dispersed in the continuous amorphous matrix.^[22] This difference can be explained

with the higher degree of unsaturation of both SBR and CBR as compared to IIR, producing larger number of chemical cross-links between the c-IPN components and hence, reducing the extent of phase separation.

Figure 2c,d shows STEM images of the same samples and their energy-dispersive X-ray spectroscopy (EDX) maps where the elemental distributions for carbon (C) and oxygen (O) atoms are shown in red and blue, respectively, while overlapping C (red) and O atoms (blue) appear purple. Because only PC18A component of the c-IPNs contains O atoms, the images also support the

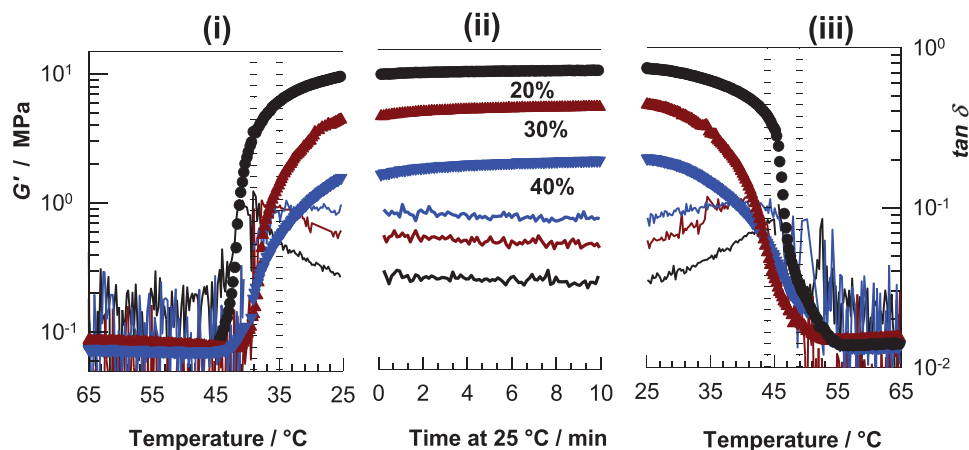


Figure 3. G' (symbols) and $\tan \delta$ (curves) of c-IPNs with 20 to 40 wt% NR-2 rubber during a thermal cycle composed of 3 steps, namely i) cooling from 65 to 25 °C at a rate of 2 °C min⁻¹, ii) isothermal at 25 °C for 10 min, and iii) heating back to 65 °C at the same rate. $\gamma_0 = 0.1\%$. $\omega = 6.3 \text{ rad s}^{-1}$. The ranges of T_m and T_{cry} of c-IPNs are indicated by the dotted vertical lines.

spatial distribution of their components over the whole examined area. We have to note that the TEM images of c-IPNs prepared using natural rubber NR-1 were blurry and had low contrast for the visualization of the particles (Figure S5, Supporting Information).

3.2. Viscoelastic Properties

All c-IPNs exhibited a significant temperature sensitivity in their viscoelastic and mechanical properties when the temperature is changed between below and above T_m and T_{cry} of their PC18A component. **Figure 3** shows the variation of the storage modulus G' (symbols) and loss factor $\tan \delta$ ($= G''/G'$, where G'' is the loss modulus) of c-IPN specimens with various NR-2 contents during a thermal cycle composed of 3 steps, namely i) cooling from 65 to 25 °C at a rate of 2 °C min⁻¹, ii) isothermal at 25 °C for 10 min, and iii) heating back to 65 °C at the same rate. The cycles are completely reversible during which G' changes by one to two orders of magnitude at the transition temperatures T_m and T_{cry} , as indicated by the dotted vertical lines. The extent of the modulus variation increases with decreasing rubber content; for instance, G' of the c-IPN with 20 wt% NR-2 is 10 MPa and 76 kPa at 25 and 65 °C, respectively, revealing a 132-fold change in its stiffness. Such a drastic and reversible variation of the modulus depending on the temperature is required for a highly efficient shape-memory effect. An interesting observation from **Figure 3** is that, although the modulus G' drastically decreases upon heating above T_m , the loss factor $\tan \delta$ also decreases. Because $\tan \delta$ represents the ratio of dissipated to stored energy during a sinusoidal loading, decrease in $\tan \delta$ above T_m means that c-IPNs in molten state possess a higher elastic character than in semicrystalline state. This unexpected behavior was also observed by frequency-sweep tests conducted at below and above T_m (**Figure 4a,b**).

Figure 4a,b shows frequency (ω) dependence of the dynamic moduli G' and G'' (filled and open symbols, respectively), and $\tan \delta$ (curves) of c-IPNs with 30 wt% CBR, NR-2, and IIR at 25 (a, left

panel) and 65 °C (b, right panel). The data for all c-IPNs with various rubber contents are compiled in **Figure S6**, Supporting Information. G' of c-IPNs decreases over all frequencies when heated above T_m , the extent of which depends on the type of rubber (**Figure 4c**). c-IPNs prepared using SBR exhibit a small change in G' depending on the temperature as compared to the other rubbers which is attributed to their high chemical cross-link density reducing the flexibility of the network chains (**Figure 5c**). Moreover, ω -dependence of G' exhibits a power law behavior, $G'(\omega) \propto \omega^n$, over 2 decades ($\approx 1\text{--}100 \text{ rad s}^{-1}$) indicating the existence of temporary cross-links in c-IPNs. These temporary cross-links with finite lifetimes can be attributed to the hydrophobic associations between noncrystalline C18 side chains contributing more than 70% of the total side chains (**Figure 1c**). As will be discussed in the next section, crystalline domains and hydrophobic associations serving as physical cross-links constitute a significant fraction of the total cross-link density of c-IPNs. Moreover, the power law exponent n differs at below and above T_m , as compiled in **Figure 4d**. For c-IPNs with NR-2, SBR, and CBR, the exponent n decreases from around 0.03 to 0.01 upon heating from 25 and 65 °C, revealing a lower frequency dependence and increasing lifetime of cross-links above T_m . A similar result can be seen when the loss factor $\tan \delta$ of c-IPNs is compared below and above T_m (the solid curves in **Figure 4a,b**). $\tan \delta$ significantly decreases above T_m indicating their increasing elastic response. The only exception is the c-IPNs based on IIR exhibiting a higher $\tan \delta$ and n above T_m (**Figure 4a–c**). Thus, c-IPNs containing NR-2, SBR, and CBR become a more elastic material with longer cross-link lifetimes in the molten state as compared to their semicrystalline state. These observations can be explained with the coexistence of chemical cross-links, and crystalline domains acting as physical cross-links. Upon heating above T_m , c-IPNs turn into purely chemically cross-linked ones with elastic behavior due to the melting of crystalline domains. As will be discussed in the next section, c-IPNs containing IIR have a much lower chemical cross-link density than the other rubbers. As a consequence, they exhibit the usual viscous character in the molten state.

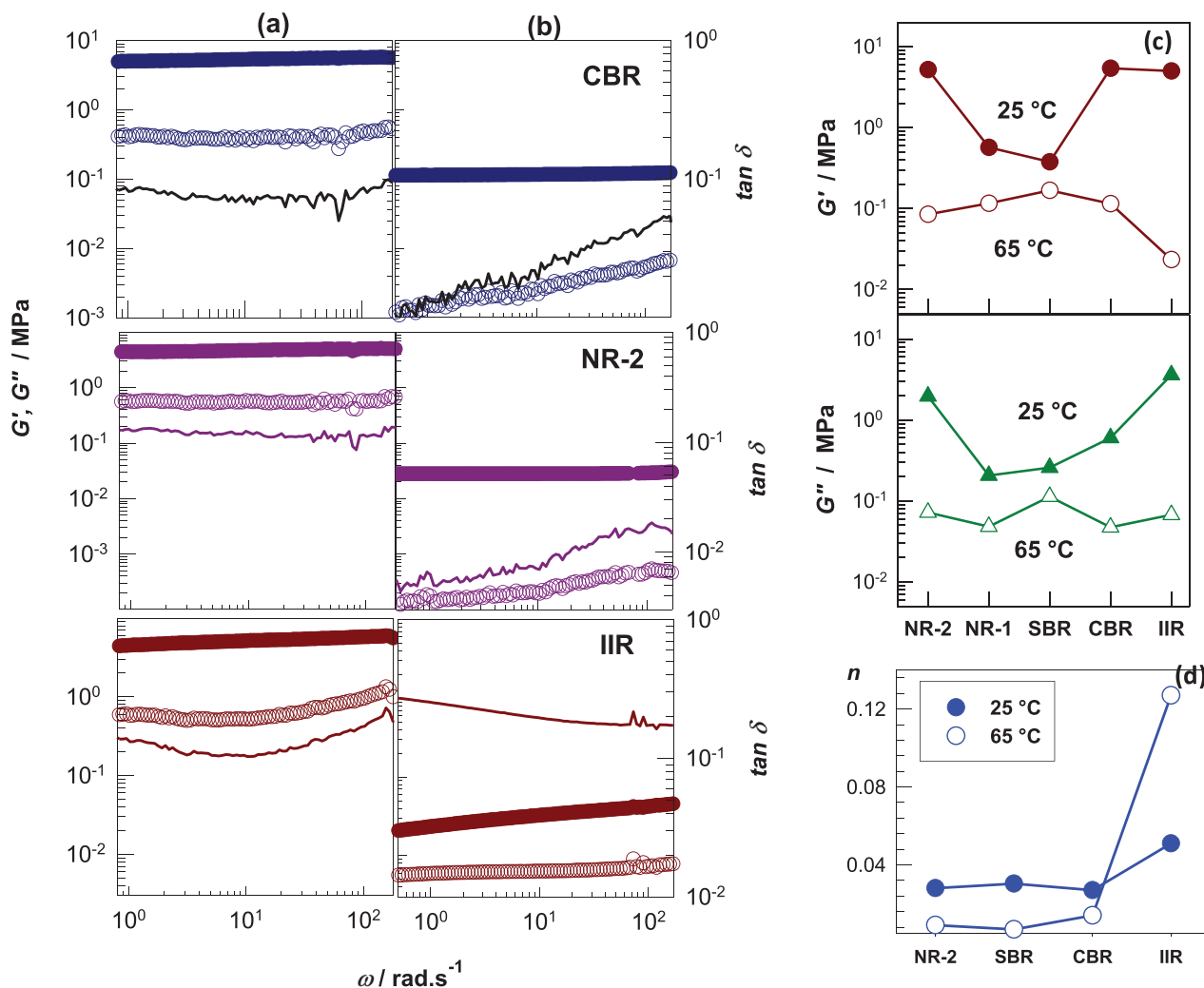


Figure 4. Frequency (ω) dependences of G' (filled symbols), G'' (open symbols) and $\tan \delta$ (curves) of c-IPNs with 30 wt% rubber at a) 25 and b) 65 °C. The type of rubbers as indicated. $\gamma_0 = 0.1\%$. c) G' and G'' measured at $\omega = 6.28 \text{ rad}\cdot\text{s}^{-1}$, and d) the exponent n for c-IPNs at 25 (filled symbols) and 65 °C (open symbols) for various rubbers.

3.3. Effective Chemical Cross-Link Density of c-IPNs

During the polymerization of C18A monomer in the presence of rubber, the growing PC18A radicals may attack to the unsaturated units of the rubber chains to form chemical cross-links. To compare the chemical cross-link density of c-IPNs prepared with different rubbers, we conducted swelling and solubility measurements in toluene which is a good solvent for their components. The crystalline domains and hydrophobic associations acting as physical cross-links are known to dissociate upon swelling of c-IPNs in toluene resulting in only chemical cross-links in the c-IPN structure.^[25–28] Figure 5a,b shows the equilibrium weight swelling ratio q_w and soluble fraction w_{sol} for c-IPNs, respectively, plotted against the type of the rubbers used in their preparation. IIR rubber produces c-IPNs with the highest swelling ratio and soluble fraction as compared to the other rubbers. This qualitatively reflects the low chemical cross-link density $v_{e,\text{chem}}$ of IIR-based c-IPNs. One may also estimate $v_{e,\text{chem}}$

using the equilibrium swelling theory of Flory and Rehner by the equation,^[29]

$$v_{e,\text{chem}} = \frac{-\left[\ln(1 - \phi_2) + \phi_2 + \chi(\phi_2)^2\right]}{V_1 \left[\phi_2^{1/3}(\phi_2^0)^{2/3} - \phi_2/2\right]} \quad (1)$$

where ϕ_2 and ϕ_2^0 are the volume fractions of chemically cross-linked polymer in equilibrium swollen and as-prepared states, respectively, which are related to q_w and w_{sol} by $\phi_2 = (1 - w_{\text{sol}})d_1/(\rho q_w)$ and $\phi_2^0 = (1 - w_{\text{sol}})$, χ is the polymer-solvent interaction parameter, ρ and d_1 are the densities of c-IPN, and toluene, and V_1 is the molar volume of toluene. Using the densities and χ parameter values reported in the literature (Table S1, Supporting Information), the calculated chemical cross-link densities $v_{e,\text{chem}}$ are shown in Figure 5c by the open symbols. Moreover, assuming affine network behavior, the total cross-link density v_e of c-IPNs

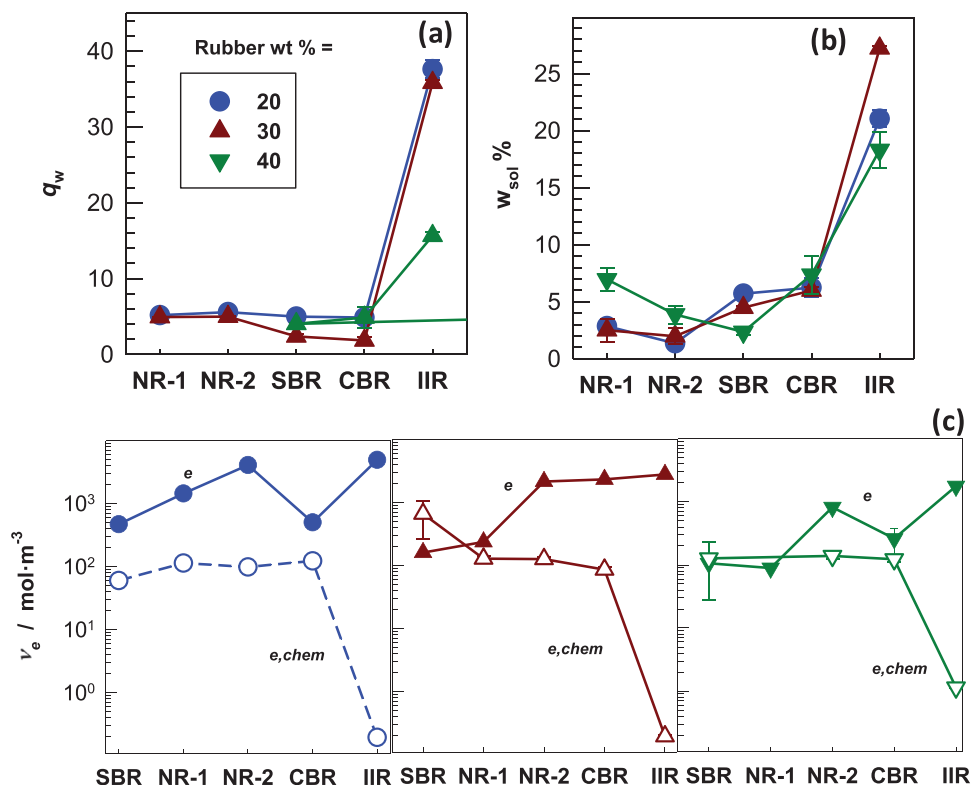


Figure 5. a,b) The equilibrium weight swelling ratio q_w and soluble fraction w_{sol} of c-IPNs plotted against the type of rubber. c) Chemical $v_{e,chem}$ (open symbols), and total cross-link densities v_e (filled symbols) of c-IPNs containing various rubbers. Rubber contents are (from left): 20, 30, and 40 wt%.

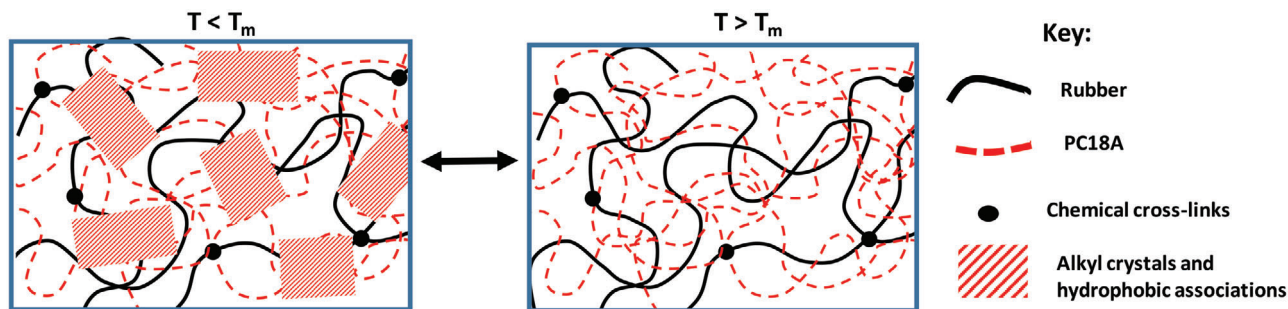


Figure 6. Scheme showing the types of cross-links in c-IPNs at below and above T_m .

can be estimated from their shear modulus at below T_m . Taking the storage modulus measured at 25 °C and $\omega = 6.28 \text{ rad s}^{-1}$ as equal to the shear modulus, one may estimate v_e as,^[29–31]

$$v_e = \frac{G'}{R T \phi_2^2} \quad (2)$$

where R is the gas constant and T is the absolute temperature. The filled symbols in Figure 5c present the total cross-link density v_e of c-IPNs at various rubber contents.

In accord with the swelling and solubility test results, the contribution of the chemical cross-link density $v_{e,chem}$ to the total cross-link density v_e is very low for c-IPNs containing IIR. In contrast, all other rubbers with a high degree of unsaturation

produce c-IPNs possessing a significant number of chemical cross-links. For instance, they exhibit two to three orders of magnitude higher chemical cross-link density $v_{e,chem}$ than those containing IIR (Figure 5c). These findings also explain why all c-IPNs except those containing IIR become more elastic when heated above their melting temperature. As schematically illustrated in Figure 6, at $T < T_m$, c-IPNs contain chemical cross-links together with alkyl crystals and hydrophobic association acting as physical cross-links so that they exhibit a high storage modulus. The presence of physical cross-links also contributes to their viscous behavior so that $\tan \delta$ remains at around 0.1. However, when heated above T_m , the physical cross-links disappear so that a pure chemically cross-linked c-IPN network forms with lesser viscous behavior.

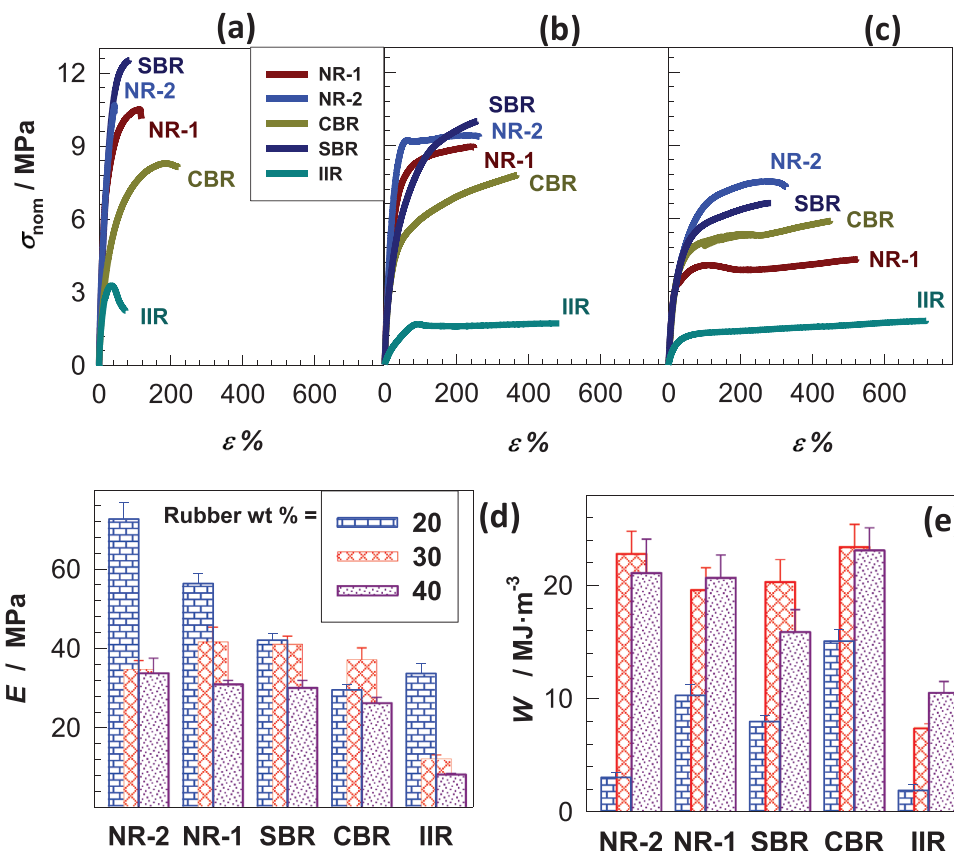


Figure 7. Tensile stress strain curves of c-IPNs with a) 20, b) 30, and c) 40 wt% rubber. The dependences of d) Young's modulus E , and e) toughness W of c-IPNs on the type of the rubber. The rubber contents are indicated.

3.4. Mechanical Properties and Shape-Memory Function

Uniaxial tensile tests were conducted on c-IPNs at 23 ± 2 °C at a fixed strain rate of 5 min^{-1} . **Figure 7a–c** shows tensile stress strain curves of c-IPNs with 20, 30, and 40 wt% rubber, respectively, as the dependence of the nominal stress σ_{nom} on the strain ϵ . The mechanical parameters are compiled in **Figure 7d,e**, and **Figure S7**, Supporting Information, where Young's modulus E , toughness W , fractures stress σ_f , and elongation to break σ_f are shown for various rubber components. The general trend is that, the rubbers with a higher unsaturation degree as compared to IIR produce c-IPNs with a high modulus and toughness. Moreover, increasing the rubber content from 20 to 30 wt% induces a brittle-to-ductile transition in their mechanical behavior. The results also show that the mechanical parameters can be tuned over a wide range by changing the type of rubber. For instance, the modulus E and toughness W of c-IPNs could be varied between 8.3 ± 0.3 – 73 ± 4 MPa, and 1.9 ± 0.5 – 23 ± 2 MJ·m⁻³, respectively, by changing the amount and the type of the rubber component. Moreover, the highest stretchability of $735 \pm 42\%$ was reached using IIR, as expected due to its low chemical cross-link density.

Cyclic mechanical tests were conducted on c-IPNs to examine the recoverability of the microstructural damage during deformation. **Figure 8a–c** shows the results of cyclic tensile tests for c-IPNs with 30 wt% SBR, CBR, and IIR, respectively. The tests

were conducted up to a maximum strain of 60% without a waiting time between cycles. The solid black and blue curves represent the 1st and 2nd loading curves while the dotted curves represent unloading ones. All c-IPNs exhibit irreversible deformation, that is, the 2nd loading follows a different path from the 1st loading indicating the occurrence of a microscopic damage in the specimens that cannot be recovered after unloading. The hysteresis energies U_{hys} calculated from the area between the loading and unloading curves also show a significant decrease after the first cycle (**Figure 8d**). To determine the self-recoverability of c-IPNs, damaged c-IPN specimens after the first cycle was heated to 65 °C for 15 min (above T_m) to reorganize the crystalline domains and hydrophobic associations and then cooled below T_m . The so repaired specimens were then subjected to a next tensile cycle. The results are shown in **Figure 8a–c** by the dashed red curves. All c-IPNs except IIR-based ones are not recoverable as expected from the existence of a large number of chemical cross-links. Indeed, cut-and-heal tests revealed no heating-induced healing in c-IPNs except the IIR containing ones. This can be attributed to their relatively high chemical cross-link densities diminishing the healing ability. Crystalline domains fragmented under strain could not be repaired after the heat treatment due to the steric effect of the chemical cross-links hindering the alignment of PC18A chains to recover the virgin microstructure.

In contrast, however, all c-IPNs exhibited an efficient shape-memory function with complete shape-fixity and shape-recovery

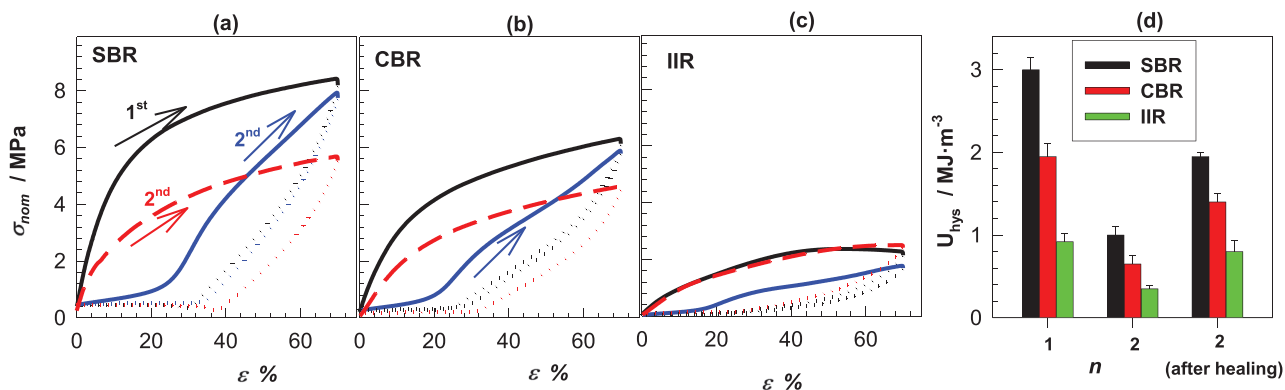


Figure 8. Cyclic tensile test results for c-IPNs containing 30 wt% a) SBR, b) CBR, and c) IIR, respectively. The solid black and blue curves represent the 1st and 2nd loading curves while the dotted curves represent unloading ones. The dashed red curves are the 2nd loading curves after heat treatment. d) U_{hys} of c-IPNs plotted against the number of cycles n .

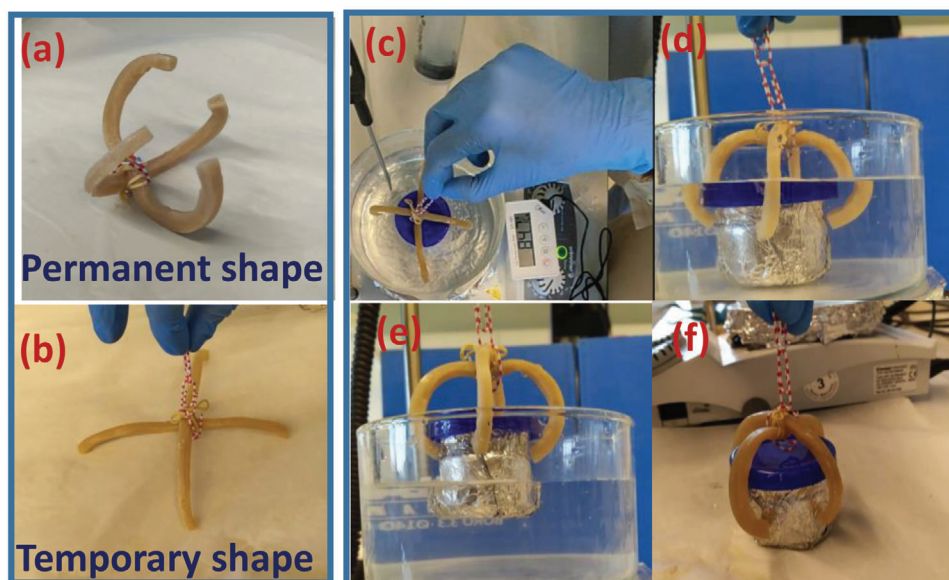


Figure 9. The images of a c-IPN specimen with 30 wt% NR-2 in a) closed-, and b) open-hand forms, and c-f) its application as a robotic gripper that grabs an object of 72 g in mass.

ratios. For instance, **Figure 9a,b** shows the images of a four-fingered hand shaped c-IPN specimen in its permanent and temporary shapes, respectively. The chemical cross-links in the c-IPN determine its permanent closed-hand form (a) while alkyl crystals fix its temporary open-hand form (b). The shape (b) is obtained by heating the specimen in its permanent shape above T_m , reshaping it to the open-hand form, followed by cooling below T_m to fix the temporary shape. The specimen in the temporary shape recovers its permanent shape at 85 °C within 15 s. **Figure 9c–f** shows the application of the c-IPN specimen as a robotic gripper that can grab an object of 72 g in mass. The robotic gripper grabs the object in a water bath at 85 °C due to the recovery its permanent shape and brings it out of water. **Figure 10** shows the shape-recovery ratio R_θ of c-IPNs as a function of temperature. The specimens in their temporary U-shape recover their original rod-shape in a small range of temperature at around 50 °C which is almost independent on their rubber contents.

Before concluding we should discuss the suitability of the term “interconnected interpenetrating polymer network” (c-IPN) that we used throughout the manuscript to describe the polymeric materials based on rubber and PC18A. As detailed above, the cross-linking reactions between the unsaturated units of the rubber and the growing PC18A radicals during the photopolymerization of C18A monomer lead to the formation of a chemically cross-linked rubber network interconnected with PC18A chains (**Figure S8a**, Supporting Information). Moreover, a second network of PC18A chains also forms by intermolecular physical cross-links, namely by crystalline domains and hydrophobic associations (**Figure S8b**, Supporting Information). Such physical networks based on PC18A have already been reported from our laboratory.^[27,32–34] Considering the fact that the total cross-link density of the materials is mainly determined by their physical cross-link density (**Figure 5c**), PC18A network has a much higher cross-link density than the rubber network. Thus, the present

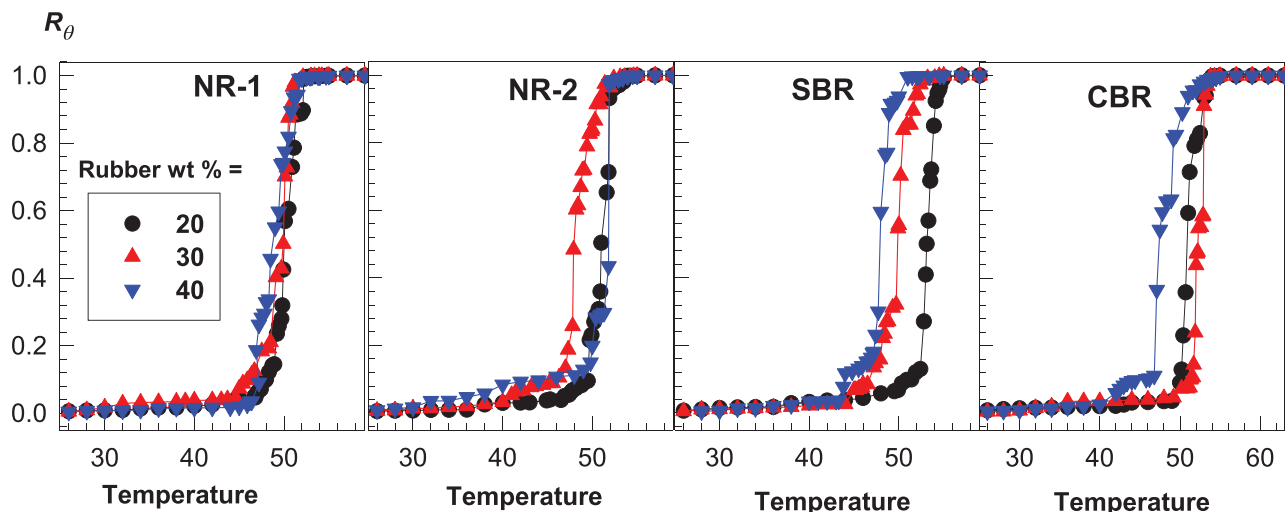


Figure 10. The shape-recovery ratio R_θ of c-IPNs plotted against the temperature. The type of rubbers and their amounts are indicated.

materials can be named as c-IPNs as illustrated in Figure S8c, Supporting Information presenting interconnected interpenetrating rubber and PC18A networks. It might be argued that the rubber chains are interconnected by short branches of C18A oligomers to form a branched rubber network. We determined the molecular weight of PC18A component by conducting UV polymerization of C18A under the same experimental condition but in the absence of rubber.^[22] The results of GPC analysis show that the number-average molecular weight of PC18A is 90 000 g mol⁻¹ with a very broad polydispersity index of 20, which is likely due to phase separation of crystalline C18A segments. Another proof for the formation of c-IPN structure is the degree of crystallinity f_{cry} of the materials, which is the mole fraction of C18A segments involved in crystalline domains (Figure 1c). f_{cry} varies between 5% and 27% depending on the type and amount of the rubbers indicating that 73% to 95% of C18A segments are part of the amorphous phase together with the rubber chains. Thus, interconnected interpenetrating rubber and noncrystalline PC18A networks constitute the nanosized amorphous particles which are interconnected by the phase separated crystalline PC18A segments.

4. Conclusions

Generating shape-memory function in commercially available and widely used rubbers draw much attention in recent years for numerous applications including smart medical devices and flexible electronics. We recently reported a simple strategy for producing interconnected IPNs based on IIR and semicrystalline PC18A exhibiting high self-healing and shape-memory efficiencies. The aim of the present study was to understand how the degree of unsaturation of the commercial rubber affects the thermal and mechanical properties, and smart functions of c-IPNs. Experiments were conducted using NR, CBR, and SBR rubbers having a much higher unsaturation degree than IIR. Dissolution of the rubbers in C18A monomer containing a photoinitiator followed by UV polymerization at 30 ± 2 °C leads to the formation of c-IPNs possessing crystalline domains. They exhibit T_m and

T_{cry} between 45–50 and 35–40 °C, respectively, that can be tuned by the amount and the type of the rubbers. The morphology of c-IPNs consists of amorphous nanoparticles of around 64 nm diameter composed of interconnected noncrystalline PC18A and rubber networks, surrounded by crystalline PC18A segments. All c-IPNs exhibit a significant temperature sensitivity in their viscoelastic and mechanical properties when the temperature is changed between below and above T_m and T_{cry} . Moreover, c-IPNs above T_m with a low stiffness (kPa level) exhibit a more elastic character than those below T_m with a high stiffness (MPa level) due to the presence of both chemical and physical cross-links. Calculations indicate that the chemical cross-link density of c-IPNs is much higher than those based on IIR, which is explained with the difference in the degree of unsaturation of the rubbers. All c-IPNs exhibit tunable mechanical properties, for example, their Young's modulus and toughness could be varied between 8.3–73 MPa, and 1.9–23 MJ m⁻³, respectively, by changing the amount and type of the rubber. Because of the coexistence of chemical cross-links and crystalline domains acting as the net-points and switching segments, respectively, c-IPNs exhibit an efficient shape-memory function with complete shape-fixity and shape-recovery ratios. This behavior was demonstrated in their potential application as a robotic gripper in the form of a four-fingered hand.

Supporting Information

Supporting Information is available from the Wiley Online Library or from the author.

Acknowledgements

This work was supported by the Scientific and Technical Research Council of Turkey (TUBITAK), MAG-218M502. O.O. thanks the Turkish Academy of Sciences (TUBA) for the partial support.

Conflict of Interest

The authors declare no conflict of interest.

Data Availability Statement

The data that support the findings of this study are openly available in the Supporting Information of this article.

Keywords

interconnected-interpenetrating polymer networks, rubbers, semicrystalline polymer, shape-memory

Received: October 16, 2021
Revised: December 17, 2021
Published online: January 2, 2022

-
- [1] *Self-Healing Materials* (Eds: M. D. Hager, S. van der Zwaag, U. S. Schubert) Springer, Berlin **2016**.
- [2] *Self-Healing and Self-Recovering Hydrogels* (Eds: C. Creton, O. Okay), Springer, Berlin **2020**.
- [3] M. Behl, A. Lendlein, in *Shape-Memory Polymers*, Springer, Berlin **2010**.
- [4] X. Zang, Y. He, Z. Fang, X. Wang, J. Ji, Y. Wang, M. Xue, *Macromol. Mater. Eng.* **2020**, *305*, 1900581.
- [5] X. Q. Feng, G. Z. Zhang, Q. M. Bai, H. Y. Jiang, B. o Xu, H. J. Li, *Macromol. Mater. Eng.* **2016**, *301*, 125.
- [6] X. Kuang, K. Chen, C. K. Dunn, J. Wu, V. C. F. Li, H. J. Qi, *ACS Appl. Mater. Interfaces* **2018**, *10*, 7381.
- [7] M. Hernández Santana, M. Den Brabander, S. García, S. Van Der Zwaag, *Polym. Rev.* **2018**, *58*, 585.
- [8] A. Das, A. Sallat, F. Böhme, M. Suckow, D. Basu, S. Wießner, K. W. Stöckelhuber, B. Voit, G. Heinrich, *ACS Appl. Mater. Interfaces* **2015**, *7*, 20623.
- [9] M. Suckow, A. Mordvinkin, M. Roy, N. K. Singha, G. Heinrich, B. Voit, K. Saalwächter, F. Böhme, *Macromolecules* **2018**, *51*, 468.
- [10] A. C. Schüssele, F. Nübling, Y. i Thomann, O. Carstensen, G. Bauer, T. Speck, R. Mühlaupt, *Macromol. Mater. Eng.* **2012**, *297*, 411.
- [11] S.-M. Lai, J.-L. Liu, Y.-H. Huang, *J. Macromol. Sci., Part B: Phys.* **2020**, *59*, 587.
- [12] Y. Cao, Y. J. Tan, S. Li, W. W. Lee, H. Guo, Y. Cai, C. Wang, B. C.-K. Tee, *Nat. Electron.* **2019**, *2*, 75.
- [13] Y.-W. Chang, in *Functional Polymer Blends. Synthesis, Properties, and Performance* (Ed: V. Mittal), CRC, Taylor & Francis Group, Boca Raton **2012**, Ch. 4.
- [14] K. Yu, A. Xin, Z. Feng, K. H. Lee, Q. Wang, *J. Mech. Phys. Solids* **2020**, *137*, 103831.
- [15] V. Montano, M. M. B. Wempe, S. M. H. Does, J. C. Bijleveld, S. Van Der Zwaag, S. J. Garcia, *Macromolecules* **2019**, *52*, 8067.
- [16] C. Xu, J. Nie, W. Wu, Z. Zheng, Y. Chen, *ACS Sustainable Chem. Eng.* **2019**, *7*, 15778.
- [17] H. H. Le, S. Hait, A. Das, S. Wiessner, K. W. Stöckelhuber, F. Boehme, Uta Reuter, K. Naskar, G. Heinrich, H.-J. Radsch, *eXPRESS Polym. Lett.* **2017**, *11*, 230.
- [18] M. A. Rhaman, M. Penco, G. Spagnoli, A. M. Grande, L. Di Landro, *Macromol. Mater. Eng.* **2011**, *296*, 1119.
- [19] J.-C. Kim, Y.-W. Chang, M. Sabzi, *Eur. Polym. J.* **2011**, *152*, 110488.
- [20] M. Kashif, Y.-W. Chang, *Eur. Polym. J.* **2015**, *70*, 306.
- [21] J. Du, D. Liu, Z. Zhang, X. Yao, D. Wan, H. Pu, Z. Lu, *Polymer* **2017**, *126*, 206.
- [22] E. Su, C. Bilici, G. Bayazit, S. Ide, O. Okay, *ACS Appl. Mater. Interfaces* **2021**, *13*, 21786.
- [23] Z. Mogri, D. R. Paul, *Polymer* **2001**, *42*, 2531.
- [24] H. S. Bishr, P. P. Pande, A. K. Chatterjee, *Eur. Polym. J.* **2002**, *38*, 2355.
- [25] A. Matsuda, J. Sato, H. Yasunaga, Y. Osada, *Macromolecules* **1994**, *27*, 7695.
- [26] Y. Osada, A. Matsuda, *Nature* **1995**, *376*, 219.
- [27] C. Bilici, V. Can, U. Nöchel, M. Behl, A. Lendlein, O. Okay, *Macromolecules* **2016**, *49*, 7442.
- [28] Y. Yang, C. Wang, C. G. Wiener, J. Hao, S. Shatas, R. A. Weiss, B. D. Vogt, *ACS Appl. Mater. Interfaces* **2016**, *8*, 22774.
- [29] P. J. Flory, *Principles of Polymer Chemistry*, Cornell University Press, Ithaca, NY **1953**.
- [30] L. R. G. Treloar, *The Physics of Rubber Elasticity*, University Press, Oxford **1975**.
- [31] J. E. Mark, B. Erman, *Rubberlike Elasticity*, Cambridge University Press, Cambridge **2007**.
- [32] O. Okay, *Self-Healing Hydrogels Formed via Hydrophobic Interactions*, Springer, Berlin **2015**.
- [33] C. Bilici, S. Ide, O. Okay, *Macromolecules* **2017**, *50*, 3647.
- [34] B. Kurt, U. Gulyuz, D. D. Demir, O. Okay, *Eur. Polym. J.* **2016**, *81*, 12.